PNAS RESEARCH ARTICLE | APPLIED BIOLOGICAL SCIENCES

High-sensitivity, protein-independent detection of dsDNA sequences

Jiaqi Yan[a,b,c], Rajendra Bhadane[d], Wentao Xu[a], Meixin Ran[b,e], Xiaochao Ma[b,e], Yuanqiang Li[b,e], Kevin Jahnke[a,f], Xiaodong Ma[b,e], Outi M. H. Salo-Ahen[b,g], Mauri A. Kostiainen[h], David A. Weitz[a,1], and Hongbo Zhang[b,c,e,1]

Affiliations are included on p. 10.

Edited by Egbert (Bert) Meijer, Technische Universiteit, Eindhoven, Netherlands; received July 8, 2025; accepted December 12, 2025

Current methodologies for detecting the sequence of double-stranded DNA (dsDNA) require amplifying and denaturing the target into single-stranded DNA (ssDNA) to enable sequence detection through Watson–Crick base pairing. However, these approaches are limited by the risks of nonspecific amplification, reliance on complex, temperature-sensitive protein enzymes, and harsh reaction conditions, such as in strong base or acidic environments. Here, we introduce a dsDNA detection platform that integrates a peptide nucleic acid (PNA) as the dsDNA denaturation agent, with multicomponent deoxyribozyme as the ssDNA detection tool, in a droplet-based system. This protein- and amplification-free method offers single-nucleotide resolution, detects down to a single dsDNA molecule, and delivers results within 1 h at room temperature. This work introduces a conceptually unique approach, that may be useful for both diagnostics and therapeutics.

peptide nucleic acid | multicomponent deoxyribozyme | microfluidics | double-stranded DNA | sequence detection

Significance

Accurate and efficient detection of target gene sequences is fundamental to genetic diagnostics and research. Compared to single-stranded sequence, double-stranded sequence detection is significantly more challenging due to its stable duplex structure. Current methods often rely on complex enzymatic reactions to separate and amplify these double-strands for analysis, which can cause errors and complicate workflows. This study introduces an enzyme-free, amplification-independent approach that combines γPNA with multicomponent DNAzymes (MNAzymes, composed solely of DNA) in a droplet-detection system. The method achieves single-nucleotide resolution and attomole sensitivity for analyzing plasmids and cellular fragments, providing a precise, accessible, and efficient platform for any double-stranded nucleic acid.

Biomarker detection is a fundamental tool in diagnostics, widely employed for disease diagnosis, prognosis, risk assessment, and monitoring therapeutic efficacy (1). Among the various biomolecular targets, genomic double-stranded DNA (dsDNA) stands out as the most direct and reliable indicator for identifying dsDNA-based pathogens. Compared to mRNA or protein, dsDNA offers distinct advantages for early pathogen identification, because they often precede antibody production or the appearance of clinical symptoms. Detection of dsDNA is also essential for identifying mutations in circulating tumor DNA, which are critical for tumor genetic diagnosis, recurrence monitoring, and guiding personalized treatments, such as detecting epidermal growth factor receptor (EGFR) mutations to inform lung cancer therapy (2). Additionally, dsDNA testing offers the most precise method for diagnosing genetic diseases, including targeted region sequencing and single nucleotide polymorphism (SNP) analysis (3), which can identify mutations responsible for conditions like albinism, progeria, and thalassemia.

The detection of DNA sequences relies on the principle of complementary nucleic acid recognition (4, 5). Many simple and rapid methods are available for detecting single-stranded DNA (ssDNA) because ssDNA readily binds to detection tools through Watson–Crick base pairing (6). However, detecting dsDNA is more challenging, as the strands must first be unwound to expose the target sequence as ssDNA. There are, however, several suitable methods for detecting dsDNA. For example, PCR (7) is highly sensitive and widely used, and is the gold standard method for amplifying and detecting dsDNA sequences. However, it requires specialized thermal cyclers (8) to denature and anneal dsDNA, and relies on enzymes that are sensitive to storage and transport. The CRISPR-Cas12 system (9) offers high dsDNA specificity through precise single-guide RNA (sgRNA) targeting and excellent signal amplification. However, its reliance on the Cas12 protein (10) for dsDNA unwinding and the requirement for a protospacer adjacent motif (PAM) (11) sequence introduce challenges in storage and handling while limiting its applicability to specific target sequences. Multicomponent deoxyribozyme (MNAzyme) systems amplify signals (12–15) with high sensitivity, making them effective for detecting ssDNA targets. However, for dsDNA detection, they depend on strong alkali solutions (pH >13) to unwind dsDNA, followed by acid neutralization (pH < 1) and stabilization with complex blocking strands (16). The harsh chemical treatments and complex strand designs make this approach challenging for practical use. Therefore, each of these methods achieve dsDNA unwinding in different ways, but each suffers limitations including dependence on high temperatures and enzymes, instability and sequence-specific requirements, or reliance on harsh chemical treatments and complex designs.

Author contributions: J.Y., D.A.W., and H.Z. designed research; J.Y., R.B., W.X., M.R., X.M., Y.L., and X.M. performed research; O.M.H.S.-A., D.A.W., and H.Z. contributed new reagents/analytic tools; J.Y. and R.B. analyzed data; and J.Y., K.J., M.A.K., D.A.W., and H.Z. wrote the paper.

Competing interest statement: Åbo Akademi University has filed a patent on the composition and methods for target sequence detection in dsDNA by using PNA/MNAzyme combination.

This article is a PNAS Direct Submission.

[1]To whom correspondence may be addressed. Email: weitz@seas.harvard.edu or hongbo.zhang@abo.fi.

This article contains supporting information online at https://www.pnas.org/lookup/suppl/doi:10.1073/pnas.2515765123/-/DCSupplemental.

Published February 4, 2026.

Beyond the unwinding difficulties, current detection technologies rely on preamplification to achieve lower detection limits. However, both thermal cycling PCR (17) and isothermal methods like loop-mediated isothermal amplification (LAMP) and recombinase polymerase amplification (RPA) are prone to nonspecific amplification (18). Additionally, these approaches involve complex protein enzymes and intricate designs. To address these issues, it is essential to develop an enzyme- and amplification-free technology that can rapidly and efficiently recognize specific dsDNA sequences at mild conditions.

In this study, we present a protein enzyme-independent droplet technology for detecting dsDNA sequences with single-nucleotide resolution. This system enables rapid, amplification-free sequence detection at the single-molecule level under room-temperature conditions. All components are stable for storage and transport in ambient environments.

Specifically, we introduce γPNA to selectively unwind dsDNA, exposing target sequences as ssDNA. We employ a MNAzyme to precisely detect target ssDNA sequences. By optimizing the ratio of γPNA to MNAzyme, we develop an optimal detection formula for dsDNA samples. Additionally, we refine the length of the MNAzyme's binding arms, achieving the detection of single-base mutations. Subsequently, we establish a γPNA/MNAzyme droplet-based system, which concentrate detection signals within picoliter droplets, enabling a single-molecule detection limit as low as 5 aM. To construct the γPNA/MNAzyme droplet system, we address three key challenges. First, we find γPNA sequences similar to the target gene can weakly trigger MNAzyme substrate cleavage, but we identify an optimal detection period to minimize false signals. Second, even when γPNA and the MNAzyme are coadministered to plasmid DNA, γPNA still invades the duplex, permitting their codelivery without mutual interference. Finally, by integrating droplet technology, we enhance the detection limit from 500 fM to the aM level.

Results

The MNAzyme is composed of three main components: biomarker-binding arms (BBAs), a catalytic core, and substrate-recognition arms. In the presence of a biomarker (the ssDNA to be detected, $ssDNA^{d}$) and a metal cofactor, the MNAzyme self-assembles to cleave a substrate (FAM-BHQ1 fluorescence probes) (19). This cleavage generates fluorescent signal, enabling the detection of the biomarker (Fig. 1*A*). To confirm the detection ability of MNAzyme to dsDNA, we investigate whether γPNA can unwind dsDNA, and further help MNAzyme recognize and bind with sequence of interest, and mediating substrate cleavage (Fig. 1 *A* and *C*). We focus on whether γPNA alone mediates MNAzyme cleavage of its substrate, causing false signals (Fig. 1*B*). Ca^{2+} is used as the metal cofactor for MNAzyme. Plasmid containing the target sequence is used as the dsDNA sample (Fig. 1*C*), while the sequence in dsDNA that is fully complementary to γPNA is named $ssDNA^{fc}$, and the corresponding sequence to be detected is named $ssDNA^{d}$.

The macroscopic results (after 12 h reaction) reveal that Groups 3 and 4, which contain the plasmid and γPNA (with different Ca^{2+} concentrations), exhibit strong detection signals (Fig. 1*D*). In contrast, Group 5, lacking the plasmid, produces no signals. These results suggest that γPNA hybridizes with the plasmid, exposing $ssDNA^{d}$ for MNAzyme combination, and facilitating MNAzyme-mediated cleavage of the fluorescent substrate. More importantly, γPNA alone does not activate MNAzyme.

Similarly, we investigate the ability of γPNA to facilitate MNAzyme detection of dsDNA from a molecular perspective using polyacrylamide gel electrophoresis (PAGE). The lanes represent various combinations of plasmid, γPNA, MNAzyme, substrate (Sub), and Ca^{2+} as indicated in the table below the gel (Fig. 1*E*). The labels on the right (plasmid, M + S, S, P) correspond to the observed bands, indicating the plasmid, MNAzyme/substrate complex, substrate, cleaved product, respectively (Fig. 1*E*). As anticipated, the group with γPNA and plasmid (Group 4) facilitate MNAzyme cleavage of the substrate after a 12 h reaction. Surprisingly, γPNA is found to slightly activate MNAzyme for substrate cleavage, however, with low efficiency (Group 6).

This phenomenon is crucial for determining whether γPNA can be used for MNAzyme-mediated dsDNA detection. Therefore, we compare the abilities of plasmid ($ssDNA^{d}$) and γPNA to catalyze the MNAzyme cleavage of the substrate. The lanes correspond to reaction times ranging from 0 to 240 min, labeled above the gel, as shown in Fig. 1 *F* and *G*. The bands on the gel represent the plasmid (high molecular weight), the MNAzyme/substrate complex (M + S), the cleaved product (P), and a complex between the MNAzyme and one half of the cleaved substrate (M + P) (Fig. 1*F* and *SI Appendix*, Fig. S1*A*). Molecular weight markers on the left indicate fragment sizes in base pairs. The results show that within 2 h of reaction, plasmid mediates nearly 100% substrate cleavage, with detectable cleaved substrate signals within 30 min (Fig. 1*F*). In contrast, γPNA only mediates less than 5% substrate cleavage within 4 h (Fig. 1*G*). Comparing the pseudo-first-order rate constant (k_{obs}), we find that plasmid-mediated catalysis occurs 4,400 times faster than that of γPNA (Fig. 1*H*). Hence, for a 30 min to 2 h reaction period, γPNA aids MNAzyme in dsDNA detection without generating false signals. Therefore, within a 2 h incubation period (sufficient for conducting the test), γPNA does not activate MNAzyme.

The double-helix structure of DNA relies on two key interactions: stacking interactions between the bases along the helix and hydrogen bonding forces between complementary base pairs (20). γPNA has the same base composition as DNA, while its structural backbone is different. The catalytic mechanism of MNAzyme primarily relies on the correct spatial structure of its catalytic core. When γPNA binds to the BBAs, if the binding mechanism aligns with the traditional double helix structure, MNAzyme will form the proper catalytic loop conformation, enabling the cleavage of the substrate fluorescent sequence. Conversely, if the interaction between γPNA and BBAs results in a different structure from the conventional double helix, the catalytic activity of MNAzyme will be significantly affected (*SI Appendix*, Fig. S1 *B*–*E*). This structural variance will lead to changes in catalytic activity.

Therefore, we combine MNAzyme with $ssDNA^{d}$ or γPNA to construct two models, and explore the differences in binding strength and spatial motion trajectories between the two models (named as DNA/MNAzyme and γPNA/MNAzyme) using molecular dynamics (MD) (21). ssDNA or γPNA is presented in orange color in Fig. 2 *A* and *B*. Following 100 ns of MD simulation, significant changes are observed in the spatial arrangement of the γPNA and ssDNA sequences when integrating with MNAzyme. First, the γPNA orients itself in a V shape when it binds to MNAzyme at the BBAs site, whereas the ssDNA forms a typical right-handed helix with W shape (Fig. 2*C*). These differences can be attributed to differences in binding interactions, as evidenced by the stronger Pi–Pi stacking observed in the γPNA/MNAzyme structure than that in the DNA/MNAzyme structure (Fig. 2*C*). Second, unlike the ssDNA system, the angle between γPNA and the substrate is large, resulting in the positioning of partzyme (blue and green strand) approximately on the same side of the plane (Fig. 2*D*). Third, by examining the difference in the end-to-end distance (22) between DNA and γPNA, we observe that at 100 ns,

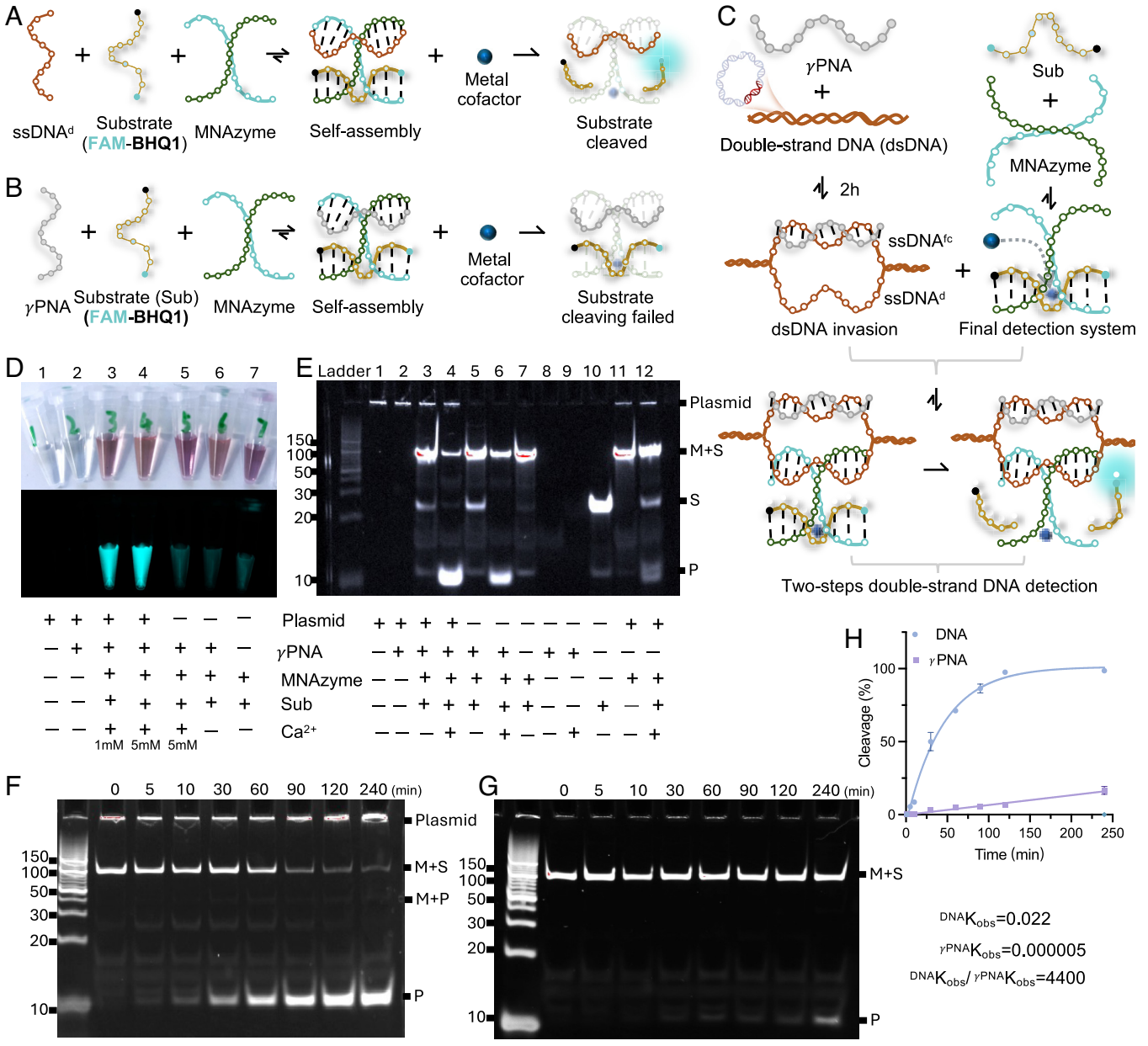

Fig. 1. Two-step dsDNA detection via MNAzyme self-assembly and cleavage mechanism. (*A*) Illustration of the MNAzyme assembly and cleavage process using a ssDNA target. The presence of the target and a metal cofactor enables MNAzyme self-assembly, which cleaves the substrate (FAM-BHQ1) and generates a fluorescent signal. (*B*) Illustration showing the failure of substrate cleavage when γPNA replaces the ssDNA target. (*C*) Diagram of the two-step dsDNA detection system. γPNA invades dsDNA to bind with fully complementary strand (ssDNAfc), to release a complementary ssDNAd target, which then activates the MNAzyme, leading to substrate cleavage and signal generation. (*D*) Images of reaction tubes under normal/fluorescence light, showing fluorescence changes under different reaction conditions. The table below details the components included in each reaction. (*E*) Gel electrophoresis results for various reaction setups, demonstrating the dependency of substrate cleavage on the presence of the plasmid, MNAzyme, substrate, and Ca^{2+}. Bands represent plasmid, MNAzyme/substrate complex (M + S), substrate (S), and cleaved product (P). (*F*) Time-course gel electrophoresis showing the gradual cleavage of the substrate to produce the product over 240 min in the presence of plasmid. (*G*) Time-course gel electrophoresis showing substrate cleavage in the presence of γPNA instead of plasmid. (*H*) Kinetic analysis of substrate strand cleavage by MNAzyme in (*F*) and (*G*) is conducted. Data points represent the percentage of substrate cleavage. The concentrations of γPNA, plasmid, MNAzyme, and substrate in (*D*–*H*) are as follows: γPNA = 2 μM, Plasmid = 100 nM, MNAzyme = 100 μM, Substrate = 100 μM.

the γPNA distance is approximately 53 to 57 Å, while the DNA system distance is approximately 65 Å (Fig. 2 *E* and *F*), indicating that γPNA sequence is more compact. Additionally, through persistence length (p) calculations (23), we notice that γPNA is more flexible, with a P-value of 8.6 Å (Å), which is less than that of the DNA system (p = 10.9 Å) (*SI Appendix*, Fig. S2).

Structural alterations can impact the atomic positions of the catalytic core adjacent to the BBAs within MNAzyme, influencing its catalytic activity. To assess the mobility of the atoms within the catalytic core of MNAzyme, we calculate the Rms fluctuation (RMSF) (24) of each atom within the catalytic core (Fig. 2*G*). The RMSF values of the catalytic core atoms near the BBAs are significantly higher in the γPNA/MNAzyme system (purple dots) than in the DNA/MNAzyme system (blue dots). This outcome suggests deformation in the catalytic core of γPNA/MNAzyme, affecting the spatial configuration required for the formation of an active catalytic environment.

We further enlarge the representation of the MNAzyme structure to observe each base within the catalytic core more clearly. The catalytic core of the DNA/MNAzyme system exhibits a uniform double-helical structure, with each base facing inward toward the core (Fig. 2*H*). However, in the γPNA/MNAzyme system, the

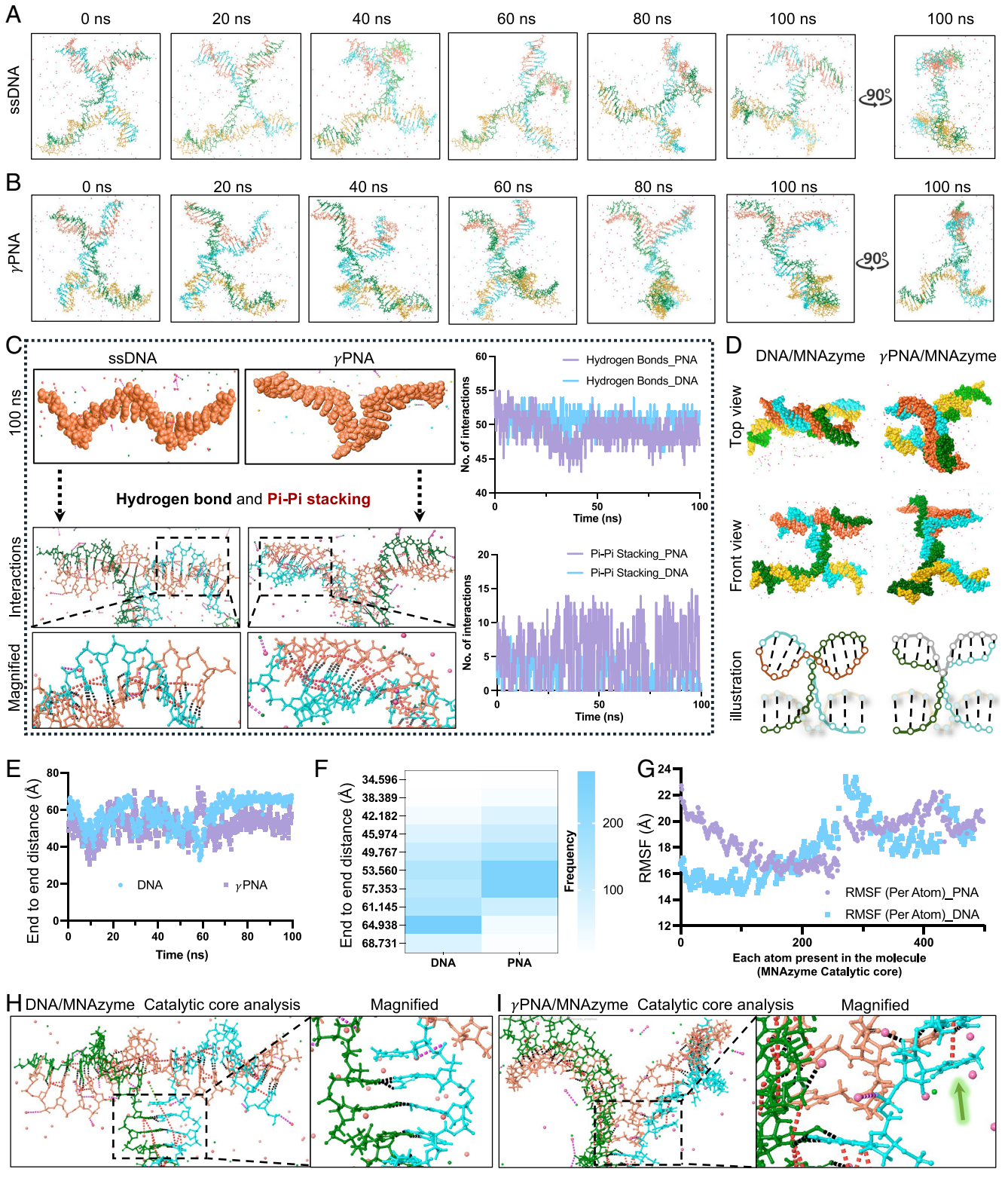

Fig. 2. Structural comparison between γPNA/MNAzyme and DNA/MNAzyme systems and the mechanism of action. (*A*) Trajectory images at different time intervals for the DNA/MNAzyme system. (*B*) Trajectory images at different time intervals for the γPNA/MNAzyme system. (*C*) The spatial orientation of DNA and γPNA at 100 ns, along with their interactions with the BBAs. (*D*) *Top* and *Front* views of DNA/MNAzyme and γPNA/MNAzyme, along with illustration showing differences in the representation of MNAzyme. (*E*) The polymer chain analysis calculations showing end-to-end distances with respect to simulation time for DNA and γPNA. (*F*) The end-to-end distances with respect to frequency of occurrence for DNA and γPNA during 100-ns molecular dynamics (MD) simulation. (*G*) The Rms fluctuation (RMSF) for each atom within the catalytic core of MNAzyme. The atoms from 1 to 260 denote the right Partzyme, starting from the end nearest to the BBA and extending to the farthest end. Atoms 261 to 489 denote the left Partzyme, starting from the end farthest from the BBAs and extending to the nearest end. (*H*) The spatial structure of the catalytic core within the DNA/MNAzyme system. (*I*) The spatial structure of the catalytic core within the γPNA/MNAzyme system. The bases within the catalytic core are pushed outward by the inserted γPNA, as indicated by the green arrows. The orange strand signifies the γPNA or DNA biomarker sequence. The green and blue strands represent the two Partzyme. The black dashed lines denote hydrogen bonds, while the purple dashed lines indicate Pi–Pi base stacking forces. Purple spheres represent calcium ions, and green spheres represent chloride ions.

V-shaped γPNA is inserted into the interior of the catalytic core, causing the bases near the BBAs to get pushed outward (Fig. 2*I*). This steric hindrance effect suggests that the catalytic ring structure within the γPNA/MNAzyme system is partially disrupted, reducing its catalytic activity.

These simulation results are promising, indicating that even if the γPNA and the ssDNA share the same sequence, the γPNA theoretically will not easily activate the MNAzyme. Consequently, when utilizing γPNA and the MNAzyme to detect dsDNA, γPNA can be first added to specifically unwind the dsDNA at the target region. Following this, a greater excess (compared to the γPNA concentration) of MNAzyme can be added to bind to the exposed $ssDNA^{d}$, to activate the MNAzyme catalyzing activity, and to cleave the predesigned fluorescent labeled substrate strand (*SI Appendix*, Fig. S1 *C* and *D*).

γPNA is widely used in gene editing systems because it does not interfere with the function of gene editing tools, but often requires preincubation with dsDNA (25–27). Therefore, we initially preincubate γPNA with dsDNA for 2 h to ensure efficient invasion. However, longer invasion times lead to longer detection times. To optimize this process, we investigate the minimum preincubation time required (*SI Appendix*, Fig. S3*A*). PAGE validation experiments are conducted, where the substrate sequence is labeled with FAM alone and visible as cyan. Surprisingly, no differences are observed in the results between skipping the preincubation of γPNA with MNAzyme and incubating for 2 h, as both cases result in complete substrate cleavage. This phenomenon indicates that when γPNA and MNAzyme are added to the dsDNA sample simultaneously, MNAzyme does not affect the ability of γPNA to invade dsDNA. It is hypothesized that γPNA, after binding to the MNAzyme complex, may dissociate from the MNAzyme structure upon encountering the target $ssDNA^{fc}$. This dissociation allows γPNA to further bind to the $ssDNA^{fc}$, subsequently releasing the MNAzyme BBAs for $ssDNA^{d}$ detection (Fig. 3*A*).

To verify this, we first design two half-chain DNAs (same sequences as BBAs) and hybridize them with γPNA in a fully complementary manner. Subsequently, we add a full-chain DNA (same sequence as $ssDNA^{fc}$) that is fully complementary to the γPNA to observe whether the full chain can displace the γPNA from the two half chains or not (Fig. 3 *B*–*D*). The experiment is conducted using PAGE, with the full chain labeled with Cy5 (red signal), the two half chains labeled with FAM (green signal) (Fig. 3*E*), and the GelRed channel (*SI Appendix*, Fig. S4*A*). In Lane 4, where the full chain is combined with γPNA, new red bands appear at the top of the gel. Lane 5, where γPNA is added to the two half chains, also shows lagging green bands. In Lane 6, after preincubating γPNA with the two half chains for 30 min, then adding the full chain for 30 min, the original green lagging bands disappear and are replaced by red bands. These results demonstrate that full-length $ssDNA^{fc}$ can outcompete γPNA already bound to the two half-chain-BBAs, thereby releasing the BBAs (*SI Appendix*, Fig. S3 *B* and *C*). In addition, in the above experiment, the two half chains are perfectly split from the middle of the full chain. However, this phenomenon does not depend on the "split" point, whether it occurs in the middle of the full chain sequence or in other regions of the full chain (*SI Appendix*, Fig. S4*B*). Furthermore, when coincubating the plasmid, γPNA and the two half chains together, a large proportion of γPNA is competitively captured by the plasmid (*SI Appendix*, Fig. S4*C*).

Sufficient concentrations of γPNA, MNAzyme, and substrate are critical for enhancing detection capabilities. However, considering cost-effectiveness, we first screen the γPNA/MNAzyme system for targets at the 10 nM level. Specifically, the γPNA concentration needs to be at least twice that of the target dsDNA (e.g., 20 nM γPNA for 10 nM dsDNA) to achieve complete cleavage of the substrate by MNAzyme. When the MNAzyme and substrate are present at equimolar concentrations, this stoichiometry ensures full substrate cleavage within 2 h (*SI Appendix*, Fig. S3 *D* and *E*). Moreover, considering the multiturnover rates of MNAzyme, its concentration may be lower than that of the substrate. With at least 40 nM of MNAzyme, 200 nM of the substrate is completely cleaved within 2 h (*SI Appendix*, Fig. S3*F*). Therefore, for target dsDNA detection at concentrations below 10 nM, a combination of 20 nM γPNA, 40 nM MNAzyme, and 200 nM substrate is found to be optimal for one-step detection in a 2 h reaction system. However, when the detection time is limited, a detection time of 60 min is also effective (*SI Appendix*, Fig. S5).

Ensuring accuracy is crucial for dsDNA detection. Therefore, we further investigate the ability of the γPNA/MNAzyme system to detect single-nucleotide mutations in dsDNA sequences. The enhancement of the accuracy in MNAzyme detection of ssDNA involves altering the lengths of each left and right BBAs, with shorter arm lengths demonstrating higher accuracy (28). The shortening of one binding arm reduces its hybridization strength, making the MNAzyme more sensitive to sequence mismatches on that side. A single-nucleotide difference can thus significantly destabilize the complex and prevent cleavage, enhancing specificity without severely compromising overall stability. Thus, we initially establish the best arm-length ratio for MNAzyme in ssDNA detection and subsequently confirm the effectiveness of this ratio in dsDNA detection.

First, the BBA sequence within the MNAzyme is kept constant, while mutations are introduced into the ssDNA biomarker. Our findings indicate that when the left and right BBAs comprise 10 nucleotides, MNAzyme can accurately recognize single-base mutations only near the central core of the three nucleotides (*SI Appendix*, Fig. S6*A*). Meanwhile, adjusting the number of bases in the two BBAs to 9 and 11 enhances the catalytic activity of MNAzyme for the correct biomarker sequence, but reduces MNAzyme's ability to detect single-base mutations. (*SI Appendix*, Fig. S6*B*). Nevertheless, when the lengths of the left and right BBAs are 8 and 12 nucleotides, respectively, the shorter arm containing eight nucleotides can accurately recognize single-base gene mutations (*SI Appendix*, Fig. S6*C*).

Subsequently, we assess the capability of the premixed γPNA/MNAzyme system to detect single-base mutations in dsDNA. We keep the plasmid sequence constant and modify the BBAs of MNAzyme. This design allows us to specifically evaluate the detection precision of the MNAzyme when γPNA has already successfully invaded and opened the target dsDNA. The findings reveal that, under conditions where the γPNA is complementary to the $ssDNA^{fc}$, in contrast to the 10-10 arm MNAzyme group (*SI Appendix*, Fig. S6*D*), the 8 to 12 arm MNAzyme demonstrates a superior ability to recognize single-base mutations in the dsDNA (*SI Appendix*, Fig. S6*E*). Moreover, the precision of the γPNA/MNAzyme system is based on the dual targeting ability of γPNA and MNAzyme. Hence, when the γPNA sequence is complementary to the BBA sequence rather than that of $ssDNA^{fc}$ within the plasmid, the accuracy of plasmid dsDNA detection is enhanced (*SI Appendix*, Fig. S7).

Our findings demonstrate the efficiency of the γPNA/MNAzyme system in achieving precise one-step dsDNA detection. To further evaluate its performance, we determine the minimum detection limit of the system. The results show that the γPNA/MNAzyme system can detect plasmid concentrations as low as 500 fM (Fig. 4 *A* and *B*). However, clinical samples require the detection limit to reach the attomolar (aM) level, to ensure sensitivity suitable for detecting extremely low concentrations of sample (29–31). In fact, most current detection systems require

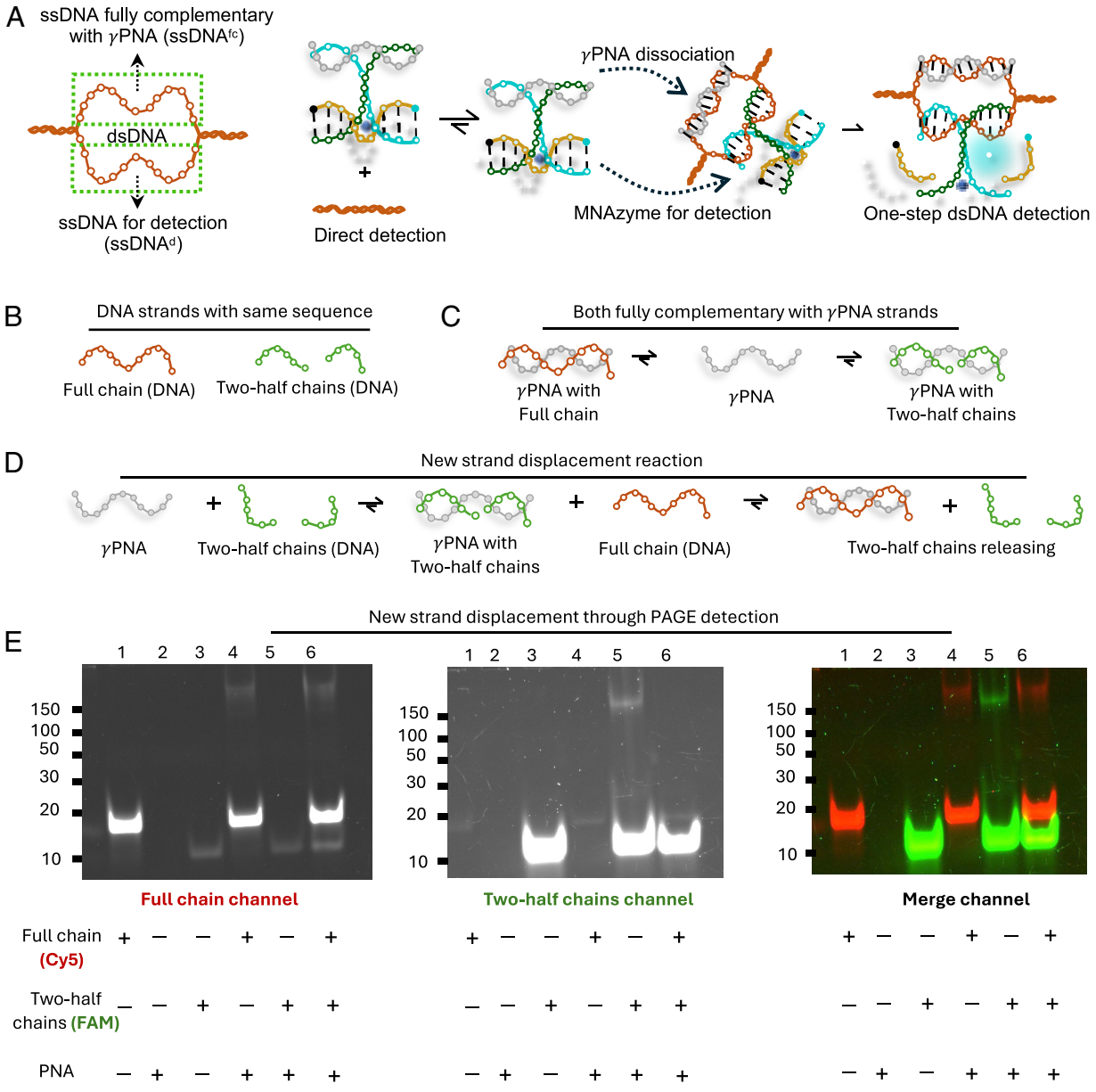

Fig. 3. Hypothesis and validation of the strand displacement reaction. (*A*) When γPNA encounters ssDNA^{fc}, ssDNA^{fc} replaces the γPNA bound to BBAs, releasing MNAzyme for the detection of ssDNA^{d}. (*B*) Two strands are prepared, including the full chain and the two half chains, the full chain and two half chains have identical sequence. (*C*) Both full chain and two half chains are fully complementary with the γPNA. (*D*) The γPNA is prebound to the two-half chains to form double strands. Subsequently, the full chain is added, and it is observed to bound to the γPNA through competition, replacing and releasing the two half chains. (*E*) Polyacrylamide gel electrophoresis (PAGE) validates the process of the new strand displacement. The full chain is labeled with Cy5, appearing red, while the two half chains are labeled with FAM, appearing green. The concentrations of the γPNA, full chain, and two half chains are 1 nM, and the reaction conditions are RNase-free.

the target sequence to be preamplified before detection. For example, CRISPR-Cas12 alone cannot achieve aM-level detection and typically relies on isothermal amplification techniques, such as RPA (32), to amplify the target for subsequent detection.

Thus, we adopted this approach, preamplifying the target plasmid or gDNA within bacteria or cells using RPA. For bacteria experiments, after plasmid extraction, two plasmids are mixed and amplified through RPA, followed by one-step detection using γPNA/MNAzyme. The results indicate that target genes extracted from bacteria are detected at a minimum concentration of approximately 5 aM using RPA and γPNA/MNAzyme synergistic detection technology (Fig. 4*C*). In the cell experiments, we mix target HeLa cells with a genome containing an enhanced green fluorescent protein (eGFP) sequence with Normal Human Dermal Fibroblasts (NHDF) cells lacking the eGFP gene, with a total cell count of 10^7. We find that the presence of a 100-target cell within 10^7 cells (1,00/10,000,000) sample is conservatively detected using fluorescence spectroscopy, PAGE, and imaging (Fig. 4*D* and *SI Appendix*, Fig. S8), achieving a detection limit of 0.1 cell/μL (100 cells/20/50 μL). However, the accuracy of this method depends primarily on gDNA extraction. In a large-cell suspension, the target gDNA can get lost; hence, the actual detection capability may be lower.

However, amplification methods such as RPA introduce multiple enzymes, including a recombinase, a single-stranded DNA–binding protein, and a strand-displacing polymerase. This complexity even limits the stability of the RPA commercial kits, which can only be stored at -20 °C for six months. Here, we

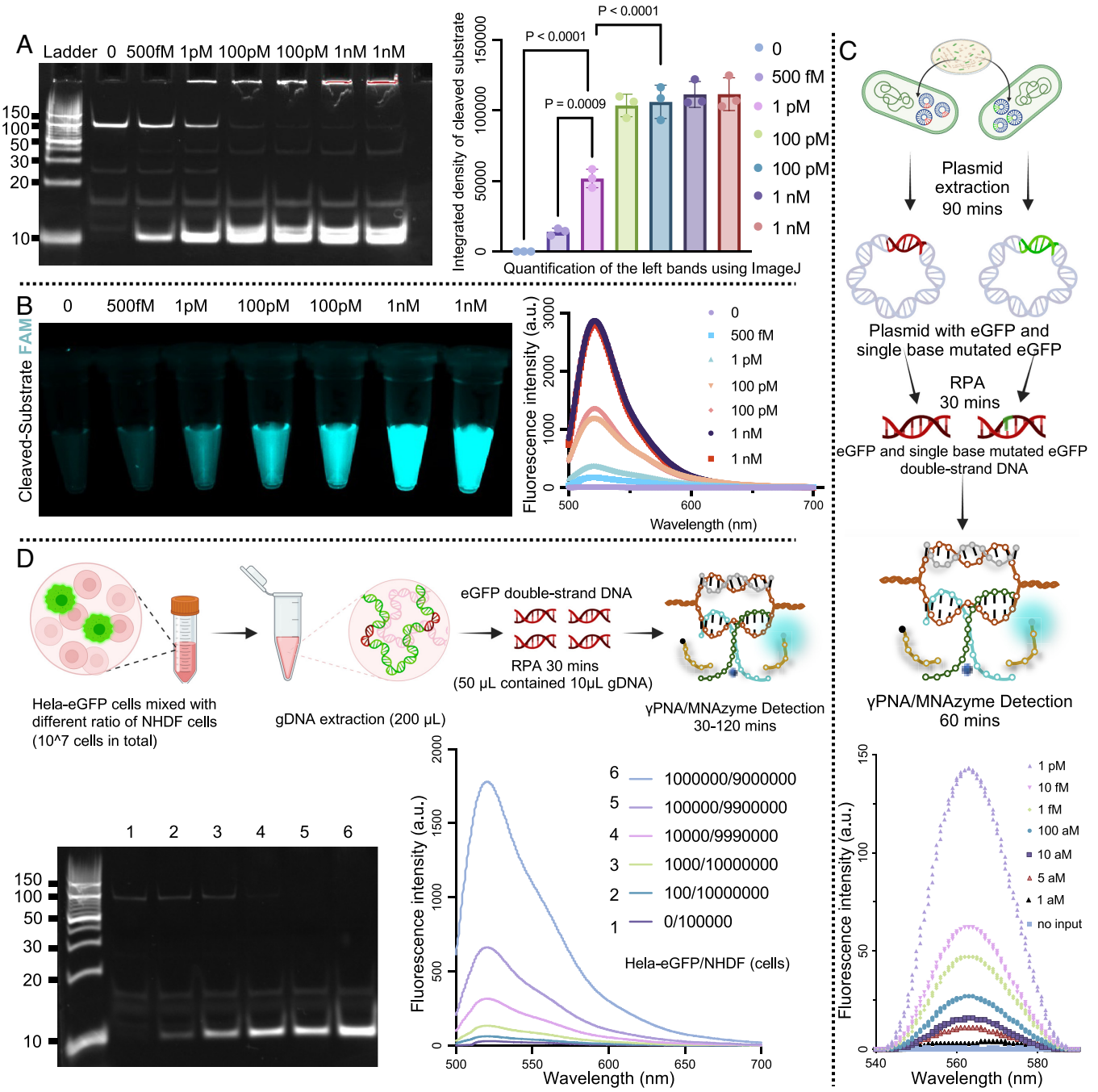

Fig. 4. Illustration of the detection limits of the γPNA/MNAzyme system and its combination with recombinase polymerase amplification (RPA) technology for dsDNA detection (*A*) PAGE is used to verify dsDNA detection at various concentrations using the γPNA/MNAzyme system. The 100 pM and 1 nM samples are run in duplicate to confirm experimental consistency. Concentrations ranged from 0 to 1 nM using plasmid dsDNA. (*B*) Macroscopic images and fluorescence spectra showing the detection system, with FAM (FAM-BHQ1) emission at 520 nm. (*C*) eGFP and single base mutated eGFP share the sample amplification primer. Target sequences within both plasmids are amplified using RPA and detected using γPNA/MNAzyme, with results represented by fluorescence spectra Cy3 (Cy3-BHQ2) at 568 nm. (*D*) Detection of target cells within a cell population using γPNA/MNAzyme is shown through PAGE and fluorescence spectra, with FAM (FAM-BHQ1) emission at 520 nm. The experimental settings include γPNA at 20 nM, MNAzyme at 40 nM, and substrate at 200 nM.

describe a method that integrates droplet microfluidics (33, 34) to achieve digital dsDNA (extracted plasmid as dsDNA example) detection with an aM detection limit, without the need for any (temperature/pH sensitive) enzyme and preamplification (Fig. 5 *A* and *B*). This approach enhances detection limits by confining fluorescence from single dsDNA molecule-mediated substrate cleavage within individual droplet, preventing signal diffusion and loss in the bulk system. The process begins by diluting the dsDNA sample and coencapsulating it with the γPNA/MNAzyme system into the water-in-oil droplets, with most droplets containing at most one dsDNA molecule (*SI Appendix*, Fig. S9). The concentrations of γPNA, MNAzyme, and the substrate are 20 nM, 40 nM, and 200 nM, respectively. After incubation at room temperature, fluorescence measurements show that in samples containing dsDNA strands (0 aM, 5 aM, 500 aM, 5 fM, 50 fM), the proportion of droplets with high fluorescence intensity increases with higher dsDNA concentrations (*SI Appendix*, Fig. S10*A*). The results indicate that in a droplet system with a diameter of 20 μm,

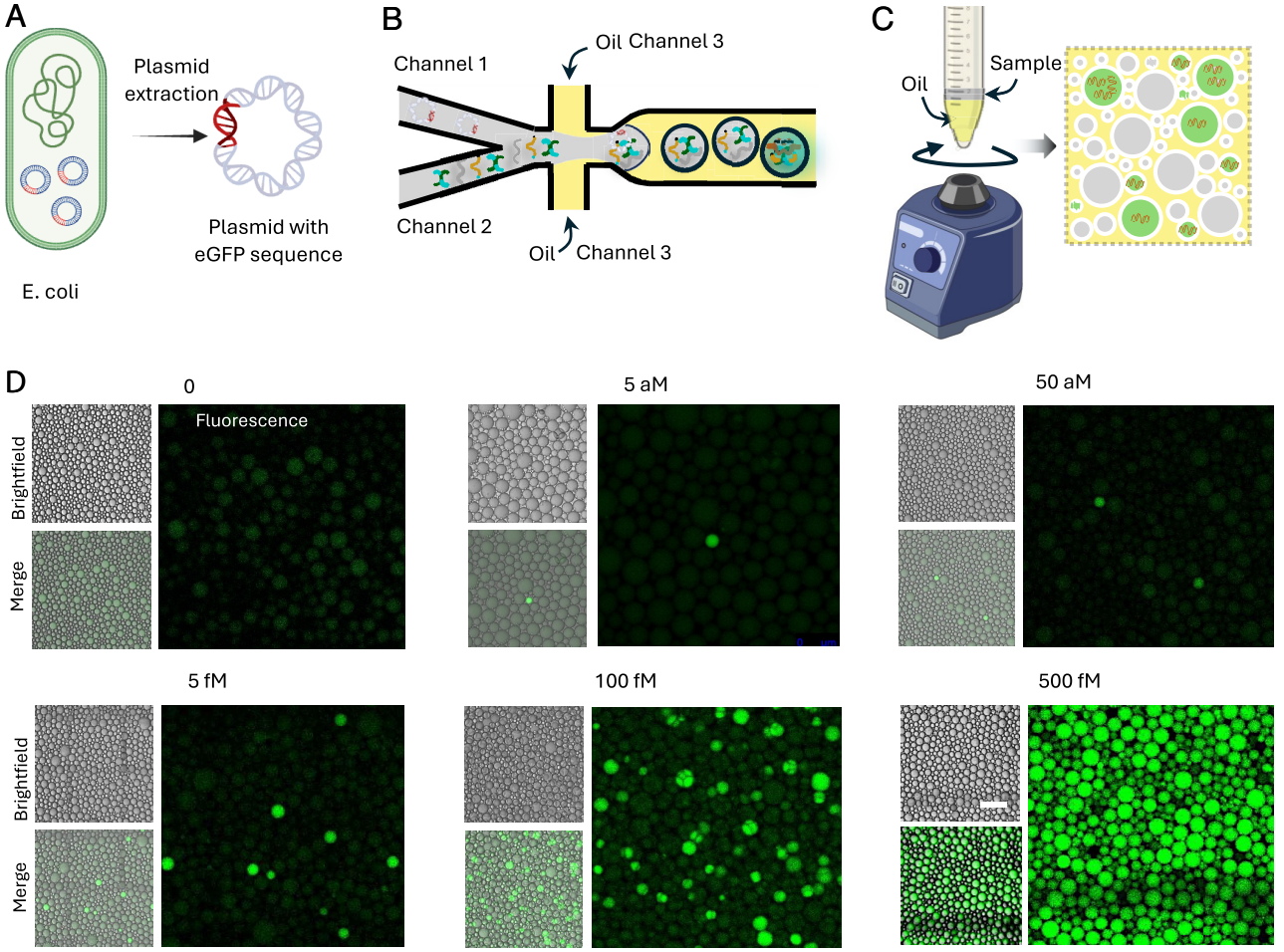

Fig. 5. Detection of plasmid DNA containing the eGFP sequence using droplet-based fluorescence analysis. (*A*) Schematic illustration of plasmid DNA extraction from *Escherichia coli*. (*B*) Microfluidic device setup for droplet generation, showing three channels: Channel 1 contains the dsDNA (plasmid) sample to be detected, Channel 2 contains the γPNA/MNAzyme system and substrate with FAM (FAM-BHQ1) emitting at 520 nm, and Channel 3 contains 2 % 008-FluoroSurfactant in HFE7500 (Ran Biotechnologies, Inc.). (*C*) Workflow for generating droplets through vortex mixing of the sample with oil. (*D*) Shaking emulsion droplet preparation results for dsDNA sample detection. (Scale bar, 120 μm.) Images showing brightfield, fluorescence, and merged views of droplets.

the proportion of bright droplets in the total droplet population follows a Poisson Distribution (*SI Appendix*, Fig. S10*B*), supporting the reliability of the detection system.

Microfluidics allows for the creation of highly uniform droplets (35), enabling precise quantitative detection of dsDNA. However, the method relies on specialized equipment and advanced technical expertise, limiting its practicality. To address this challenge, we use a shaking emulsion technique. This approach can be performed in just a few seconds using basic laboratory tools, such as a vortex mixer and tubes, to produce polydisperse droplets. By simply mixing the sample with an oil solution and shaking for 1 min, a microemulsion with droplet sizes ranging from 20 to 50 μm is generated (Fig. 5*C*). This process partitions the reaction mixtures into picoliter-scale droplets, enhancing the local concentration of cleaved substrates through the confinement effect. As demonstrated, this method allows the detection of samples with concentrations as low as ~5 aM under these conditions (Fig. 5*D*).

Discussion

In this study, we develop a γPNA/MNAzyme droplet-based system for dsDNA detection that addresses key limitations of existing methods. Without the need of protein enzymes and amplification, this system simplifies the detection process and ensures all components are stable for storage and transportation at room temperature. The incorporation of γPNA enables precise unwinding of target sequences within dsDNA under mild conditions, which allows MNAzyme to perform sequence detection with single-base resolution. As a result, this method achieves highly sensitive detection at the single dsDNA molecule level within 2 h.

PNAs can invade dsDNA without thermal denaturation (36). However, conventional PNAs often require additional structural features or are restricted to homopurine-rich target sequences to achieve effective binding (37–39). In contrast, γPNA, which incorporates a stereogenic center at the γ-position of the backbone, adopts a preorganized right-handed helical structure that significantly enhances binding kinetics and duplex stability (40). This structural advantage enables γPNA to efficiently invade dsDNA without the need for auxiliary sequences or sequence constraints. Therefore, to simplify probe design and broaden the applicability of our detection platform, we select γPNA as the strand invasion agent in this study.

Our γPNA/MNAzyme droplet dsDNA detection system has many advantages compared with current dsDNA detection technology. For example, while PCR remains the leading thermal cycling technology for dsDNA diagnostics, its reliance on specialized equipment, multiple enzymes, time-intensive protocols, skilled personnel, and susceptibility to false positives limits its broader applicability and versatility (41). More importantly, from the perspective of detection capabilities, PCR is not well-suited

for detecting sequences shorter than 40 bp (42). Furthermore, in the context of base mutation diseases and gene editing practices, such as single-base mutations/edits (43) or very short insertions (44) or deletions, traditional methods require PCR to amplify long fragments before sequencing, which is time-consuming and reduces accuracy due to repeated amplifications.

Other prominent dsDNA detection systems, including CRISPR-based systems (45), also face certain application limitations. For example, CRISPR systems rely on protein enzymes and are restricted by the requirement for protospacer adjacent motif (PAM) or protospacer flanking site (PFS) sequences (11). Additionally, some newly designed PAM-independent CRISPR systems still require the target dsDNA to have sticky ends at its termini for effective detection (46). Our γPNA/MNAzyme technology enables rapid dsDNA detection without relying on protein-based enzymes or complex machinery. Unlike advanced CRISPR-based dsDNA detection systems (Cas9 or Cas12), the γPNA/MNAzyme system is not restricted by any specific sequence, allowing it to detect all forms of target sequences in principle.

More importantly, we not only combine PNA with the ssDNA detection tool but illustrate an interesting detection mechanism. Conventionally, PNA is only used in conjunction with gene editing technologies due to its ability to specifically unwind dsDNA, enabling gene editing tools to target specific sequences within dsDNA through Watson–Crick base pairing (25–27). However, because PNA usually has an identical base sequence to the target gene, it has not been used for helping ssDNA detection tool to detect dsDNA. In this study, we challenge this conventional approach by combining PNA with the ssDNA detection tool MNAzyme. To address the issue of PNA sharing an identical base sequence with the target, we use techniques such as molecular dynamics and northern blot to determine that PNA does not inadvertently activate the detection tool, leading to false signals. Additionally, we also confirm that after PNA binds with MNAzyme, it dissociates from MNAzyme when encountering the dsDNA sample, allowing it to unwind the target gene sequence within the dsDNA. These two findings are decisive for the application of PNA in dsDNA detection, as well as for the development of future technologies in this field. Compared to PCR or various isothermal amplification techniques, our method is simpler and more straightforward.

To address nonspecific amplification caused by preamplification and the reliance on excessive protein enzymes in nucleic acid amplification, we employ microfluidic droplets and shaking emulsion droplet methods for enzyme-independent, amplification-free detection of dsDNA. In the detection of purified dsDNA samples, our method eliminates the need for expensive protein enzymes or commercial kits. It requires only mixing the sample with surfactant-containing oil and vortexing at room temperature to achieve the sample detection within droplets. Our approach achieves an ultralow detection limit, at the aM level. Other enzyme-free strategies for dsDNA detection have also been reported (47, 48), including the bio-barcode assay (49) and SERRS-based hybridization methods (50), offering alternatives to bypass the use of protein enzymes.

For future perspective, our detection technology holds potential for future applications in rapid diagnostics of various diseases. For example, it can be employed for the quick detection of dsDNA-based viruses such as Epstein–Barr virus (EBV), which is linked to long COVID and certain cancers, or Monkeypox Virus. Additionally, it can be utilized for the detection of tumor-derived circulating DNA biomarkers, *Helicobacter pylori* genotyping (associated with gastric cancer), EGFR gene mutations (related to lung cancer), and monitoring both the therapeutic efficacy and distribution of CAR-T cells during CAR-T cell treatments, all of which demand real-time diagnostic capabilities. Furthermore, our technique can also be adapted for rapidly assessing CRISPR gene-editing efficiency or for the quality control of engineered plasmid insertions or deletions.

In terms of future research directions, the use of the γPNA/MNAzyme system through more visual means offers exciting possibilities. This includes modifying the fluorescent label of the MNAzyme substrate to create a visualized quantum dot system (51) or employing lateral flow tests (52, 53) for visual detection. Moreover, with the specific binding capability of MNAzyme and PNA to dsDNA, this technology shows promise for detecting DNA methylation and other epigenetic modifications associated with various diseases. Furthermore, when applied to complex clinical samples or living cells, our system may be vulnerable to nuclease-mediated degradation. Therefore, the development of nuclease-resistant chemical modifications for MNAzymes and their substrates is a crucial direction for future optimization to enhance the robustness and broader applicability of this enzyme-free detection strategy.

Finally, the delivery of the γPNA/MNAzyme system into cells for intracellular gene diagnosis represents a groundbreaking opportunity to expand its application scope (54). Unlike the CRISPR system, γPNA/MNAzyme does not indiscriminately cut DNA fragments, thereby avoiding cellular damage. This makes it an ideal tool for nondestructive live-cell examinations, paving the way for safer and more precise diagnostics.

Materials and Methods

Design of PNA, MNAzyme. All sequences used in this work are listed in *SI Appendix*, Table S1. eGFP sequence is selected as the target dsDNA, downloaded from the SnapGene® website. Sequence Author: Clontech (Takara). The top and bottom strands of the eGFP double-stranded gene are targeted at specific diagnostic sites for the PNA design. The γPNA sequences comprise 20 bases and are purchased from PANAGENE Inc. The γPNA fragments to be tested are searched in the gene database using BLAST® to ensure sequence fidelity with the eGFP segment. Subsequent cellular detection is performed using HeLa/GFP stable cell lines (Cat# AKR-213) from Nordic BioSite Oy, which are generated by infecting the cell line with the eGFP lentivirus. The manufacturer confirms reporter expression; however, the eGFP copies integrated into the host cell genomes, and their integration positions are unknown. MNAzyme is derived from the catalytic core of 17E DNAzyme. The designed BBA corresponded to ssDNA^{d} expose after the PNA invasion. The MNAzyme sequence is purchased from Integrated DNA Technologies, Inc.

Two-Step Detection of dsDNA. During the initial validation stage, the reaction time and concentration may be longer in the subsequent stages. After incubating the plasmid with PNA for 2 h, MNAzyme and fluorescent substrate are added, and after a subsequent 12 h reaction, fluorescence imaging is conducted. For fluorescence imaging in PCR tubes, the fluorescent substrate is labeled with FAM-BHQ1, and imaging is performed using the Invitrogen iBright imaging system from Thermo Fisher.

However, for substrate cleavage analysis in the PAGE experiments, the substrate is labeled with FAM alone for easier observation. Similarly, the plasmid is first incubated with PNA for 2 h, followed by MNAzyme addition for a 12 h reaction, which is subsequently used for dsDNA detection. γPNA, plasmid, MNAzyme, and substrate concentrations are 2 μM, 100 nM, 100 μM, and 100 μM, respectively. The Ca^{2+} concentrations are 1 and 5 mM.

Kinetic Cleavage Reactions for ssDNA or PNA-Mediated Substrate Cleavage. For determining the pseudo-first-order rate constant, 1 μL from each reaction system is extracted at fixed time points and mixed with 1 μL of EDTA (0.5 M) for subsequent PAGE experiments. The bands on the PAGE gel are quantitatively analyzed using ImageJ software to obtain grayscale values. The K_{obs} values are calculated using GraphPad based on the one-phase decay model.

MNAzyme/Substrate Concentration for Single and Multiple-Turnover Plasmid Detection. After establishing the concentrations of 20 nM γPNA and 10 nM plasmid, we verify the optimal amount of MNAzyme for the Single-turnover reaction. (MNAzyme: Substrate ratio = 1:1). Although BHQ-1 in the FAM-BHQ1 fluorescence beacon can reduce the fluorescence intensity of FAM, some residual fluorescence might persist, causing an increased background signal during detection. Therefore, this study aims to determine the optimal MNAzyme dosage to cleave all substrates, minimizing interference from background signals. For the 200 nM substrate, we investigate the MNAzyme dosage under various turnover rates. The MNAzyme concentrations are 10, 40, 80, 160, and 200 nM. The reaction is conducted in nuclease-free water with a 5 mM calcium ion metal cofactor solution for 2 h. The substrate chain is labeled with FAM.

Single-Base Mutation Detection for ssDNA and dsDNA. To detect single-base mutations in ssDNA, we initially fix the MNAzyme sequence and mutate the ssDNA to be tested. In the PAGE assays, the fluorescent substrate is labeled with FAM alone. For fluorescence imaging in PCR tubes, the substrate is labeled with FAM-BHQ1. The concentrations of the ssDNA to be tested, MNAzyme, and fluorescent substrate are 10, 40, and 200 nM, respectively, with a reaction time of approximately 1 h.

To detect single-base mutations in a dsDNA, the sequence of the dsDNA is fixed, and the BBA sequences of MNAzyme are varied to validate the accuracy of MNAzyme in detecting dsDNA mutations. γPNA is initially fully complementary to the $ssDNA^{fc}$ of MNAzyme and subsequently matches with the sequence of the BBAs of MNAzyme. The detection system comprises a plasmid at a concentration of 10 nM, γPNA at 20 nM, MNAzyme at 40 nM, and FAM-labeled substrate at 200 nM, with a reaction time of 1 h. The detection system is a 10 μL reaction solution containing 5 mM calcium ions.

Detection Limit Test. To explore the detection limits, we keep the concentrations of γPNA, MNAzyme, and substrate fixed at 20, 40, and 200 nM, respectively. The concentrations of the analyzed dsDNA (plasmid) are 0, 500 fM, 1 pM, 100 pM, 100 pM, 1 nM, and 1 nM. To ensure a maximal detection signal, the detection time is set to 2 h. The detection limit is assessed by performing 20% PAGE followed by GelRed staining to quantify band grayscale values using the ImageJ software. Additionally, fluorescence imaging is conducted using PCR tubes, and fluorescence spectra are obtained using a Nanodrop™ 3300 (Thermo Fisher). The fluorescent substrate is labeled with FAM-BHQ1, and the fluorescence scanning wavelength is set between 500 and 700 nm.

Data, Materials, and Software Availability. Source Data have been deposited in Zenodo (https://doi.org/10.5281/zenodo.18291448) (55). All other data are included in the article and/or *SI Appendix*.

ACKNOWLEDGMENTS. We thank the Zhejiang Provincial Natural Science Foundation of China [BD24H180001 (H.Z.)], the Research Project [Grant No. 347897 (H.Z.)], Solution for Health Profile [Grant No. 336355 (H.Z.)], InFLAMES Flagship [Grant No. 337531 (H.Z.)], and "Printed Intelligence Infrastructure" (PIIFIRI) (H.Z.)" from Research Council of Finland; NIH/University of Pittsburgh [Grant No. R01AI153156 (D.A.W)]; and the Tor, Joe, and Pentti Borg Memorial Fund (O.S). J.Y. thanks the Finnish Culture Foundation Post Doc Pool grant. K.J. thanks the Alexander von Humboldt Foundation for financial support. We acknowledge the Academy of Finland Centers of Excellence Program (2022–2029) in Life-Inspired Hybrid Materials (LIBER) 346110 (M.A.K). We thank the Center for Nanoscale Systems (CNS) in Harvard University. We thank Electron Microscopy Laboratory, Institute of Biomedicine, University of Turku, and Biocenter Finland. Also, the Biocenter Finland Bioinformatics, CSC IT Center for Science, and Prof. Mark Johnson and Dr. Jukka Lehtonen are gratefully acknowledged for the excellent computational infrastructure at the Åbo Akademi University.

Author affiliations: [a]School of Engineering and Applied Sciences, Harvard University, Cambridge, MA 02138; [b]Pharmaceutical Sciences Laboratory, Faculty of Science and Engineering, Åbo Akademi University, Turku 20520, Finland; [c]Joint Centre of Translational Medicine, the First Affiliated Hospital of Wenzhou Medical University, Wenzhou 325000, China; [d]Institute of Biomedicine, University of Turku, Turku 20520, Finland; [e]Turku Bioscience Centre, University of Turku and Åbo Akademi University, Turku 20520, Finland; [f]Max Planck Institute for Medical Research, Bildungscampus Heilbronn, Heilbronn 74076, Germany; [g]Structural Bioinformatics Laboratory, Biochemistry, Åbo Akademi University, Turku 20520, Finland; and [h]Department of Bioproducts and Biosystems, Aalto University, Aalto FI-00076, Finland

1. O. Aubert *et al.*, Cell-free DNA for the detection of kidney allograft rejection. *Nat. Med.* **30**, 2320–2327 (2024).
2. A. Tivey, M. Church, D. Rothwell, C. Dive, N. Cook, Circulating tumour DNA – Looking beyond the blood. *Nat. Rev. Clin. Oncol.* **19**, 600–612 (2022).
3. L. Zahavi *et al.*, Bacterial SNPs in the human gut microbiome associate with host BMI. *Nat. Med.* **29**, 2785–2792 (2023).
4. S. Fu *et al.*, Bacteriophage λ exonuclease and a 5′-phosphorylated DNA guide allow PAM-independent targeting of double-stranded nucleic acids. *Nat. Biotechnol.* **43**, 1144–1155 (2025).
5. B. Koopal *et al.*, Short prokaryotic argonaute systems trigger cell death upon detection of invading DNA. *Cell* **185**, 1471–1486.e19 (2022).
6. J. H. Bae *et al.*, Single duplex DNA sequencing with CODEC detects mutations with high sensitivity. *Nat. Genet.* **55**, 871–879 (2023).
7. Anonymous, Testing pooled samples enables universal screening of congenital cytomegalovirus infection. *Nat. Med.* **30**, 952–953 (2024).
8. W. Chen *et al.*, Advancing quantitative PCR with color cycle multiplex amplification. *Nucl. Acids Res.* **52**, e81 (2024).
9. W. X. Yan *et al.*, Functionally diverse type V CRISPR-Cas systems. *Science* **363**, 88–91 (2019).
10. M. A. Katz *et al.*, Diverse viral cas genes antagonize CRISPR immunity. *Nature* **634**, 677–683 (2024).
11. F. Liu *et al.*, Electrochemical detection of ctDNA mutation in non-small cell lung cancer based on CRISPR/Cas12a system. *Sens. Actuators B Chem.* **362**, 131807 (2022).
12. J. Yan, M. Ran, X. Shen, H. Zhang, Therapeutic DNAzymes: From structure design to clinical applications. *Adv. Mater.* **35**, 2300374 (2023).
13. O. Hanpanich *et al.*, Label-free detection of HPV mRNA with an artificial chaperone-enhanced MNAzyme (ACEzyme)-based electrochemical sensor. *Biosens. Bioelectron.* **221**, 114352 (2023).
14. M. A. Abdou Mohamed *et al.*, Diagnosing antibiotic resistance using nucleic acid enzymes and gold nanoparticles. *ACS Nano* **15**, 9379–9390 (2021).
15. O. Hu *et al.*, A multicomponent nucleic acid enzyme-cleavable quantum dot nanobeacon for highly sensitive diagnosis of tuberculosis with the naked eye. *ACS Sens.* **8**, 254–262 (2023).
16. M. Saha, J. Bhattacharjee, S. A. Hussain, D. Bhattacharjee, Effect of denaturation of DNA on the molecular organization of a fluorescent dye in ultra thin films. *Mol. Cryst. Liq. Cryst.* **633**, 46–53 (2016).
17. J. Sun *et al.*, Correcting PCR amplification errors in unique molecular identifiers to generate accurate numbers of sequencing molecules. *Nat. Methods* **21**, 401–405 (2024).
18. A. Sen *et al.*, Paper-based loop-mediated isothermal amplification and CRISPR integrated platform for on-site nucleic acid testing of pathogens. *Biosens. Bioelectron.* **257**, 116292 (2024).
19. T. Ha *et al.*, Fluorescence resonance energy transfer at the single-molecule level. *Nat. Rev. Methods Primers* **4**, 21 (2024).
20. P. Yakovchuk, E. Protozanova, M. D. Frank-Kamenetskii, Base-stacking and base-pairing contributions into thermal stability of the DNA double helix. *Nucleic Acids Res.* **34**, 564–574 (2006).
21. L. Lu *et al.*, De novo design of drug-binding proteins with predictable binding energy and specificity. *Science* **384**, 106–112 (2024).
22. J. H. Yang, H. B. Brandão, A. S. Hansen, DNA double-strand break end synapsis by DNA loop extrusion. *Nat. Commun.* **14**, 1913 (2023).
23. S. Baral *et al.*, Single-chain polymerization dynamics and conformational mechanics of conjugated polymers. *Chem* **7**, 2175–2189 (2021).
24. Y.-W. Dong, M.-L. Liao, X.-L. Meng, G. N. Somero, Structural flexibility and protein adaptation to temperature: Molecular dynamics analysis of malate dehydrogenases of marine molluscs. *Proc. Natl. Acad. Sci.* **115**, 1274–1279 (2018).
25. M. Lyu *et al.*, PNA-assisted DNAzymes to cleave double-stranded DNA for genetic engineering with high sequence fidelity. *J. Am. Chem. Soc.* **143**, 9724–9728 (2021).
26. T. Marsic *et al.*, Programmable site-specific DNA double-strand breaks via PNA-assisted prokaryotic Argonautes. *Nucleic Acids Res.* **51**, 9491–9506 (2023).
27. R. Aman *et al.*, Peptide nucleic acid-assisted generation of targeted double-stranded DNA breaks with T7 endonuclease I. *Nucleic Acids Res.* **52**, 3469–3482 (2024).
28. C. Shi *et al.*, A programmable DNAzyme for the sensitive detection of nucleic acids. *Angew. Chem. Int. Ed.* **63**, e202320179 (2024).
29. J. S. Gootenberg *et al.*, Nucleic acid detection with CRISPR-Cas13a/C2c2. *Science* **356**, 438–442 (2017).
30. J. S. Gootenberg *et al.*, Multiplexed and portable nucleic acid detection platform with Cas13, Cas12a, and Csm6. *Science* **360**, 439–444 (2018).
31. J. S. Chen *et al.*, CRISPR-Cas12a target binding unleashes indiscriminate single-stranded DNase activity. *Science* **360**, 436–439 (2018).
32. S. Lu *et al.*, Fast and sensitive detection of SARS-CoV-2 RNA using suboptimal protospacer adjacent motifs for Cas12a. *Nat. Biomed. Eng.* **6**, 286–297 (2022).
33. L. Chen *et al.*, Targeted whole-genome recovery of single viral species in a complex environmental sample. *Proc. Natl. Acad. Sci.* **121**, e2404727121 (2024).
34. W. Zheng *et al.*, High-throughput, single-microbe genomics with strain resolution, applied to a human gut microbiome. *Science* **376**, eabm1483 (2022).
35. S. M. Prakadan, A. K. Shalek, D. A. Weitz, Scaling by shrinking: Empowering single-cell "omics" with microfluidic devices. *Nat. Rev. Genet.* **18**, 345–361 (2017).
36. J. Lee, I.-S. Park, E. Jung, Y. Lee, D.-H. Min, Direct, sequence-specific detection of dsDNA based on peptide nucleic acid and graphene oxide without requiring denaturation. *Biosens. Bioelectron.* **62**, 140–144 (2014).
37. N. O. Bukanov, V. V. Demidov, P. E. Nielsen, M. D. Frank-Kamenetskii, PD-loop: A complex of duplex DNA with an oligonucleotide. *Proc. Natl. Acad. Sci.* **95**, 5516–5520 (1998).
38. H. Kuhn *et al.*, Hybridization of DNA and PNA molecular beacons to single-stranded and double-stranded DNA targets. *J. Am. Chem. Soc.* **124**, 1097–1103 (2002).
39. K. Kaihatsu, R. H. Shah, X. Zhao, D. R. Corey, Extending recognition by peptide nucleic acids (PNAs): Binding to duplex DNA and inhibition of transcription by tail-clamp PNA–peptide conjugates. *Biochemistry* **42**, 13996–14003 (2003).
40. G. He, S. Rapireddy, R. Bahal, B. Sahu, D. H. Ly, Strand invasion of extended, mixed-sequence B-DNA by γPNAs. *J. Am. Chem. Soc.* **131**, 12088–12090 (2009).

41. S. Kwok, R. Higuchi, Avoiding false positives with PCR. *Nature* **339**, 237–238 (1989).
42. R. Takabatake, M. Kaneko, M. Yanagida, K. Kitta, Detection of 30 bp DNA fragments with a sensitive modified Southern blot analysis. *Biosci. Biotechnol. Biochem.* **84**, 2405–2414 (2020).
43. A. C. Komor, Y. B. Kim, M. S. Packer, J. A. Zuris, D. R. Liu, Programmable editing of a target base in genomic DNA without double-stranded DNA cleavage. *Nature* **533**, 420–424 (2016).
44. W. Cui *et al.*, A 20-bp insertion/deletion (indel) polymorphism within the CDC25A gene and its associations with growth traits in goat. *Arch. Anim. Breed.* **62**, 353–360 (2019).
45. C. Jiang *et al.*, A new anti-CRISPR gene promotes the spread of drug-resistance plasmids in *Klebsiella pneumoniae*. *Nucleic Acids Res.* **52**, 8370–8384 (2024).
46. W. Zhang *et al.*, PAM-independent ultra-specific activation of CRISPR-Cas12a via sticky-end dsDNA. *Nucleic Acids Res.* **50**, 12674–12688 (2022).
47. A. Ershova *et al.*, Enzyme-free exponential amplification via growth and scission of crisscross ribbons from single-stranded DNA components. *J. Am. Chem. Soc.* **146**, 218–227 (2024).
48. J. W. Beard, S. L. Hunt, A. Evans, C. Goenner, B. L. Miller, Mimicking a cellular crowding environment for enzyme-free paper-based nucleic acid tests at the point of care. *ACS Sens.* **9**, 5069–5080 (2024).
49. H. D. Hill, R. A. Vega, C. A. Mirkin, Nonenzymatic detection of bacterial genomic DNA using the bio bar code assay. *Anal. Chem.* **79**, 9218–9223 (2007).
50. C. Feuillie *et al.*, Enzyme-free detection and quantification of double-stranded nucleic acids. *Anal. Bioanal. Chem.* **404**, 415–422 (2012).
51. R. C. Castro, D. S. M. Ribeiro, J. L. M. Santos, Visual detection using quantum dots sensing platforms. *Coord. Chem. Rev.* **429**, 213637 (2021).
52. D. Wang *et al.*, Rapid lateral flow immunoassay for the fluorescence detection of SARS-CoV-2 RNA. *Nat. Biomed. Eng.* **4**, 1150–1158 (2020).
53. K. A. Kundrod *et al.*, An integrated isothermal nucleic acid amplification test to detect HPV16 and HPV18 DNA in resource-limited settings. *Sci. Transl. Med.* **15**, eabn4768 (2023).
54. J. Yan *et al.*, Development of aptamer-DNAzyme based metal-nucleic acid frameworks for gastric cancer therapy. *Nat. Commun.* **15**, 3684 (2024).
55. J. Yan, High-sensitivity, protein-independent detection of dsDNA sequences. Zenodo. https://doi.org/10.5281/zenodo.18291448. Deposited 18 January 2026.